Multiphysics Transients Modeling of Solid Oxide Fuel Cells: Methodology of Circuit Equivalents and Use in EMTP-Type Power System Simulation

Tian Lan and Kai Strunz

***Abstract*—Programs of the Electromagnetic Transients Program (EMTP) type have been the most popular digital simulators for emulating electromagnetic transients in power electric networks consisting mainly of rotating machinery, lines, transformers, loads, and power electronic converters. With the increasing interest in fuel cells, it would be beneficial to extend the scope of EMTP-type application to multiphysics transients as they appear, for example, in fuel cells. The concept and realization of this extension are presented in this paper. Analogies between electric, pneumatic, and thermal quantities are exploited for developing circuit models that describe currents and voltages, molar flows and pressures, and heat transfers and temperatures. It is shown how already existing libraries of network components of typical EMTP-type simulators accurately emulate the involved multiphysics phenomena of multiple energy carriers. The theoretical considerations are complemented by validation and application to combined heat and power to illustrate the value of the modeling. The studies are conducted using the program PSCAD as an example of the EMTP-type family and center on the solid oxide fuel cell.**

***Index Terms*—EMTP, equivalent circuits, fuel cells, hydrogen, multi-physics, power system modeling, power system simulation, solid oxide fuel cell (SOFC), distributed generation, multiple energy carriers, electromagnetic transients, combined heat and power (CHP).**

I. Introduction

ACCORDING to the U.S. Department of Energy (DOE), fuel cells are expected to be key elements for building a competitive, secure, and sustainable clean energy economy [1]. Solid Oxide Fuel Cells (SOFCs) convert the chemical energy of fuel into electricity and operate at temperatures in the region of 600 to 1000 °C [2], [3]. The energy conversion efficiency of SOFCs can reach up to 65%. Due to the high operating temperature, SOFCs allow internal reforming of gaseous fuel inside the fuel cell, making SOFCs very flexible in the choice of fuel, such as hydrogen, methane, and propane [4]. The applications of the SOFC vary from several watts to several megawatts [2], [3], [5]–[7]. The small-scale SOFCs can be used in applications such as the supply of power to microelectronic and communication equipment [6], [7]. At the larger scale, SOFCs are suitable for the application to Combined Heat and Power (CHP). In addition to electricity, CHP makes use of the heat contained in the high-temperature exhaust streams for functions such as residential heating, commercial heating, or further electricity generation [2], [3], [5].

Before fuel cells can be effectively utilized in power systems, it is important to study their behavior and interaction with other power system components [2]. Simulation tools are valuable for this purpose. Especially programs which allow a resource to be studied in interaction with other models of power system components, such as power electronics devices, are helpful. One such class of simulators is of the Electromagnetic Transients Program (EMTP) type [8].

EMTP-type simulators have been steadily extended to include a wide range of power electric and power electronic components and their controls, and to allow for optimization [9]–[11]. With the growing interest in fuel cells, it would be useful to model a fuel cell in the context of the EMTP, as it could then be readily integrated with relevant models of power electric and electronic systems. However, in order to be useful for studies such as the evaluation of a system's load-following response, control design, or calculation of hydrogen storage levels, a fuel cell model has to consider the pneumatic and thermal transients of the fuel cell in addition to the electric transients conventionally modeled in EMTP-type simulators.

A wide array of application-oriented models of a fuel cell was developed and applied [12]–[20]. In [12]–[15], the developed fuel cell models only consider the electric transients. In addition to the electric transients, the pneumatic transients were included in the fuel cell models presented in [16] and [17]. In [18]–[20], the effect of the thermal transients on fuel cell output voltage was investigated. Despite being useful for certain types of studies, these models do not simultaneously consider electric, pneumatic, and thermal transients. In [21], a one-dimensional model of a tubular SOFC for use in Matlab was developed. The fuel cell model presented in this paper specifically facilitates simulation in EMTP-type simulators. To accomplish this, electrical analogies for pneumatic and thermal quantities are employed to create a multi-physics, equivalent circuit representation of the fuel cell system.

An overview of the modeling concept proposed is presented in Section II. Next, the equivalent circuits for modeling electric,

Manuscript received May 26, 2016; revised September 11, 2016; accepted October 28, 2016. Date of publication April 27, 2017; date of current version November 22, 2017. Paper no. TEC-00444-2016. *(Corresponding author: Kai Strunz.)*

The authors are with the Institute of Sustainable Electric Networks and Sources of Energy, Technische Universität Berlin, 10623 Berlin, Germany (e-mail: T.lan@hotmail.com; kai.strunz@tu-berlin.de).

Color versions of one or more of the figures in this paper are available online at http://ieeexplore.ieee.org.

Digital Object Identifier 10.1109/TEC.2017.2687886

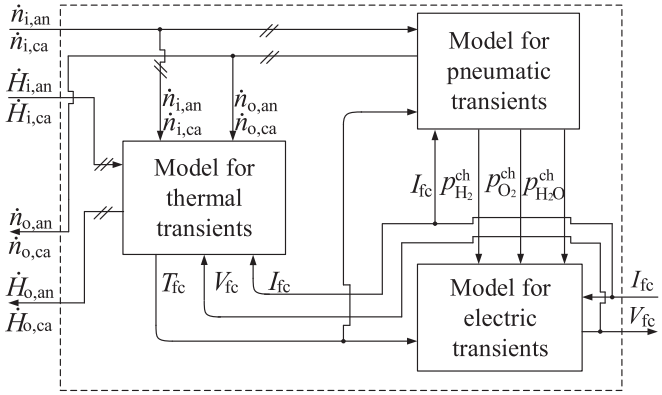

Fig. 1. Block diagram of SOFC multiphysics modeling for EMTP-type simulators.

TABLE I
EXCHANGE QUANTITIES OF MODEL OF MULTIPHYSICS TRANSIENTS

V_{fc}	terminal voltage of fuel cell stack
I_{fc}	load current of fuel cell stack
T_{fc}	temperature of fuel cell stack
$\dot{n}_{\mathrm{i,an}}, \dot{n}_{\mathrm{i,ca}}$	inlet molar flows to anode, cathode
$\dot{H}_{\mathrm{i,an}}, \dot{H}_{\mathrm{i,ca}}$	enthalpy flows affiliated with $\dot{n}_{\mathrm{i,an}}, \dot{n}_{\mathrm{i,ca}}$
$\dot{n}_{\mathrm{o,an}}, \dot{n}_{\mathrm{o,ca}}$	outlet molar flows from anode, cathode
$\dot{H}_{\mathrm{o,an}}, \dot{H}_{\mathrm{o,ca}}$	enthalpy flows affiliated with $\dot{n}_{\mathrm{o,an}}, \dot{n}_{\mathrm{o,ca}}$
$p^{\mathrm{ch}}_{\mathrm{H_2}}, p^{\mathrm{ch}}_{\mathrm{H_2O}}$	partial pressures of hydrogen and water vapor in anode channel
$p^{\mathrm{ch}}_{\mathrm{O_2}}$	partial pressure of oxygen in cathode channel

pneumatic, and thermal transients are described in Sections III–V, respectively. Section VI explains details on the integration of electric, pneumatic, and thermal transient models into a complete SOFC model in PSCAD. The model is validated for steady state and transient operation in Section VII. A test case demonstrating a possible CHP application of the model is presented in Section VIII. Conclusions are drawn in Section IX.

II. MODELING CONCEPT

Fig. 1 shows the system modeling concept. Multi-physics signal exchanges can be observed between the external and the fuel cell system, whose borders are marked by the dashed line frame. In order to emulate the different multi-physics phenomena of the fuel cell in EMTP-type simulators, equivalent circuit models to describe each of the electric, pneumatic, and thermal transients are developed. The exchange quantities shown in Fig. 1 are described in Table I.

To facilitate the modeling of the blocks of Fig. 1 in EMTP-type simulators, several assumptions are made regarding scaling, geometry, gas characteristics, and heat transfer. The list of assumptions is given in the Appendix.

III. MODELING OF ELECTRIC TRANSIENTS

In the following subsections, the electrical response of the fuel cell stack is mathematically described so as to facilitate the modeling of electrical transients with circuit elements available in EMTP-type simulators.

A. Mathematical Description

The output voltage of the fuel cell can be determined by summing the voltage contributions from the fuel cell chemical reaction, as calculated by the Nernst equation, the activation losses, the ohmic losses, and concentration losses [3]. The following subsections describe each of those as well as the electrical transient due to the double layer capacitance.

1) Nernst Voltage: The voltage produced by the chemical reaction in a fuel cell is given by the Nernst equation [2], [3]:

$$E_{\mathrm{cell}} = E_0 + \frac{\overline{R}T_{\mathrm{fc}}}{2F} \ln\left(\frac{p^{\mathrm{ch}}_{\mathrm{H_2}}\sqrt{p^{\mathrm{ch}}_{\mathrm{O_2}}}}{p^{\mathrm{ch}}_{\mathrm{H_2O}}\sqrt{p^{0}}}\right) \tag{1}$$

where E_{cell} represents the reversible voltage of a single fuel cell, $\overline{R}$ is the ideal gas constant, F is the Faraday constant, p^0 is the standard pressure, and E_0 is the cell reversible voltage at an arbitrary temperature T_{fc} and can be expressed as [2]:

$$E_0 = E^0 - k_{\mathrm{E}}(T_{\mathrm{fc}} - 298.15\ \mathrm{K}) \tag{2}$$

where k_{E} is a constant determined by experiment, E^0 is the cell reversible voltage at standard state 298.15 K and 101325 Pa. For a hydrogen-oxygen fuel cell, E^0 is 1.229 V [3].

2) Activation Voltage Drop: The fuel cell activation voltage drop is caused by the energy barrier that the reactants must overcome in the chemical reactions taking place on the surface of the electrodes. This voltage drop is nonlinear and contributes to the majority of the voltage drop during low-current fuel cell operation. The voltage drop is calculated using the Tafel equation [3]:

$$V_{\mathrm{act,cell}} = \frac{\overline{R}T_{\mathrm{fc}}}{2\alpha F} \ln\left(\frac{I_{\mathrm{fc}}}{I_0}\right) \tag{3}$$

where α is the electron transfer coefficient, I_0 is the exchange current and can be expressed as [16]:

$$I_0 = B\mathrm{e}^{\left(\frac{-W_{\mathrm{act}}}{\overline{R}T_{\mathrm{fc}}}\right)} \tag{4}$$

where B is a constant determined by experiment, and W_{act} is the activation energy of the electrochemical reaction.

The Tafel equation given by (3) only holds true when I_{fc} is larger than I_0 [3]. Therefore, according to [2], an empirical equation for $V_{\mathrm{act,cell}}$ may be expressed as follows instead of (3):

$$V_{\mathrm{act,cell}} = V_{\mathrm{act0,cell}} + V_{\mathrm{act1,cell}} \tag{5}$$

and

$$V_{\mathrm{act0,cell}} = \xi_0 + T_{\mathrm{fc}} \cdot \xi_1 \tag{6}$$

$$V_{\mathrm{act1,cell}} = \frac{\overline{R}T_{\mathrm{fc}}}{2\alpha F} \sinh^{-1}\left(\frac{I_{\mathrm{fc}}}{2I_0}\right) \tag{7}$$

where $V_{\mathrm{act1,cell}}$ is a voltage drop depending on both current and temperature, $V_{\mathrm{act0,cell}}$ includes a constant term ξ_0 and a temperature-dependent term $T_{\mathrm{fc}} \cdot \xi_1$. When the load current is zero, $V_{\mathrm{act1,cell}}$ will be zero. The voltage drop $V_{\mathrm{act0,cell}}$ defined in (6) is independent of the load current. It is included in (5) to reflect its influence on the open circuit voltage. This approach has been supported by [2].

According to assumption 1 in the Appendix, for modeling an aggregated fuel cell stack consisting of N cells, it is useful to define an open circuit voltage as follows:

$$E_{\rm oc} = N(E_{\rm cell} - V_{\rm act0,cell}) \tag{8}$$

The voltage drop $V_{\rm act1,cell}$ can be aggregated for the entire fuel cell stack and modeled as a resistance to $I_{\rm fc}$:

$$R_{\rm act} = N\frac{V_{\rm act1,cell}}{I_{\rm fc}} \tag{9}$$

3) Ohmic Voltage Drop: The ohmic voltage drop is caused by the resistance of the paths that the electrons and ions flow through. In order to calculate the nonlinear ohmic losses in the fuel cell stack, the combined resistance of the electrodes, interconnect, and the electrolyte of N cells can be lumped together and modeled as a single nonlinear resistance $R_{\rm ohm}$ [22]:

$$R_{\rm ohm} = NR_{T_\gamma}\,{\rm e}^{\left[\delta\left(\frac{1}{T_\gamma}-\frac{1}{T_{\rm fc}}\right)\right]} \tag{10}$$

$$V_{\rm ohm} = I_{\rm fc}R_{\rm ohm} \tag{11}$$

where R_{T_γ} is the ohmic resistance of a single cell at temperature T_γ, δ is a constant determined by experiment, and $V_{\rm ohm}$ is the ohmic voltage drop of the fuel cell stack.

4) Concentration Voltage Drop: The concentration voltage drop is caused by the mass transfer processes from the channels to the reaction sites in the porous electrodes. During the reaction process, mass diffusion from the flow channels to the electrode-electrolyte interface, where the reactions take place, can cause concentration gradients for the reactants. As a result, the effective partial pressures of hydrogen, oxygen, and water vapor at the reaction sites are different from those in the flow channels. To obtain the effective partial pressure for each reactant at the reaction site, it is also necessary to model the diffusion of the reactants from the anode and cathode channels through the porous electrodes. This can be accomplished using the Stefan-Maxwell formulation for the anode or cathode channel for a given reactant. For an SOFC, the Stefan-Maxwell formulation can be solved as follows for each reactant [21]:

$$p_{\rm H_2} = p^{\rm ch}_{\rm H_2} - \frac{\overline{R}T_{\rm fc}l_{\rm an}}{D_{\rm H_2,H_2O}2FA_{\rm cell}}I_{\rm fc} \tag{12}$$

$$p_{\rm H_2O} = p^{\rm ch}_{\rm H_2O} + \frac{\overline{R}T_{\rm fc}l_{\rm an}}{D_{\rm H_2O,H_2}2FA_{\rm cell}}I_{\rm fc} \tag{13}$$

$$p_{\rm O_2} = p_{\rm op} - \left(p_{\rm op} - p^{\rm ch}_{\rm O_2}\right){\rm e}^{\left(\frac{\overline{R}T_{\rm fc}l_{\rm ca}I_{\rm fc}}{D_{\rm O_2,N_2}p_{\rm op}4FA_{\rm cell}}\right)} \tag{14}$$

where $p_{\rm H_2}$, $p_{\rm O_2}$, and $p_{\rm H_2O}$ are the effective partial pressures of hydrogen, oxygen, and water vapor, respectively, at the reaction sites, $p_{\rm op}$ is the channel pressure, $D_{m,n}$ is the effective binary diffusivity of the m-n pair [19], [23], $A_{\rm cell}$ is the cell active area, and l_l is the length of the given electrode.

The concentration voltage drop is due to the concentration gradients of the reactants being transported between flow channels and reaction sites. For the aggregated fuel cell stack, it can be calculated by:

$$V_{\rm conc} = N\frac{\overline{R}T_{\rm fc}}{2F}\left[\ln\left(\frac{p^{\rm ch}_{\rm H_2}\sqrt{p^{\rm ch}_{\rm O_2}}}{p^{\rm ch}_{\rm H_2O}\sqrt{p^0}}\right) - \ln\left(\frac{p_{\rm H_2}\sqrt{p_{\rm O_2}}}{p_{\rm H_2O}\sqrt{p^0}}\right)\right] \tag{15}$$

After insertion of (12)–(14) into (15), division by fuel cell load current $I_{\rm fc}$ gives the corresponding resistance $R_{\rm conc}$:

$$R_{\rm conc} = \frac{V_{\rm conc}}{I_{\rm fc}} \tag{16}$$

5) Double Layer Charging Effect: The double layer charging effect causes an electric transient due to the buildup of charges at the electrode-electrolyte boundary layers. This effect can be modeled using an electric capacitance $C_{\rm dl}$, connected in parallel with $R_{\rm act}$ and $R_{\rm conc}$ [3] as shown in Fig. 2. Mathematically, the voltage drop $V_{\rm dl}$ across this parallel combination is represented by:

$$V_{\rm dl} = \left(I_{\rm fc} - C_{\rm dl}\frac{{\rm d}V_{\rm dl}}{{\rm d}t}\right)(R_{\rm act} + R_{\rm conc}) \tag{17}$$

6) Fuel Cell Output Voltage: Considering the voltage drops and the double layer charging effect, the output voltage of the fuel cell stack $V_{\rm fc}$ is given by the following equation:

$$V_{\rm fc} = E_{\rm oc} - V_{\rm dl} - V_{\rm ohm} \tag{18}$$

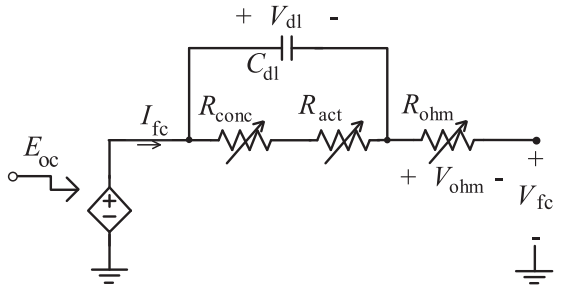

Fig. 2. Implementation of model for electric transients in PSCAD.

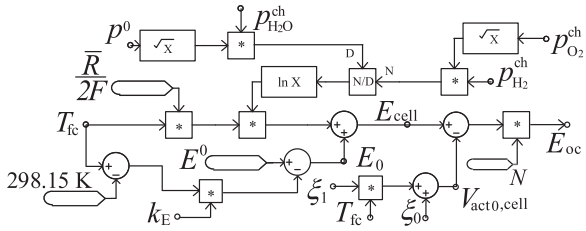

Fig. 3. Calculation of $E_{\rm oc}$ using CSMF function blocks in PSCAD.

B. Implementation

The PSCAD implementation of the model for electric transients primarily consists of the equivalent circuit model presented in Fig. 2. This circuit represents (17) and (18). All impedances are implemented as nonlinear components. The fuel cell load can be connected across $V_{\rm fc}$.

Voltage $E_{\rm oc}$ defined by (8) is evaluated using Continuous System Model Functions (CSMF) blocks from a standard PSCAD library, as shown in Fig. 3. Similarly, $R_{\rm act}$ defined by (9), $R_{\rm ohm}$ defined by (10), and $R_{\rm conc}$ defined by (16) can also be evaluated

TABLE II
ANALOGIES BETWEEN ELECTRICAL AND PNEUMATIC QUANTITIES

Quantity	Electric	Pneumatic
Potential	Voltage V (V)	Pressure p (Pa)
Flow	Current I (A)	Gas flow rate $\dot{n}$, $\dot{\nu}$ $(\mathrm{mol}\cdot\mathrm{s}^{-1})$
Capacitance	Electric capacitance C (F)	Pneumatic capacitance C_p $(\mathrm{mol}\cdot\mathrm{Pa}^{-1})$

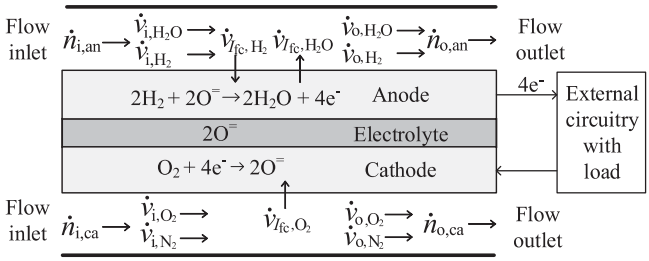

Fig. 4. Fuel cell schematic showing gas flows and chemical reactions.

using CSMF function blocks. It is noted that $p^{\mathrm{ch}}_{\mathrm{H_2}}$, $p^{\mathrm{ch}}_{\mathrm{O_2}}$, $p^{\mathrm{ch}}_{\mathrm{H_2O}}$, and T_{fc} are obtained from the models for pneumatic transients and thermal transients in Fig. 1.

The exchange current I_0 is calculated according to (4). The voltage drop $V_{\mathrm{act1,cell}}$ is calculated from (7). Since standard libraries may lack an inverse hyperbolic sine function block, the inverse hyperbolic sine in (7) is reformulated as:

$$\sinh^{-1}(x) = \ln(x + \sqrt{1+x^2}) \tag{19}$$

IV. MODELING OF PNEUMATIC TRANSIENTS

The reactant gases considered are hydrogen, water vapor, and oxygen. The output voltage characteristic of a fuel cell depends on the partial pressures of these reactant gases, as shown in Section III. This dependence necessitates the modeling of pneumatic transients inside the fuel cell, which can be accomplished in an EMTP-type simulator by utilizing well-known electrical analogies for pneumatic quantities, as described in Table II.

A. Mathematical Description

The pneumatic transients in an SOFC can be modeled by considering relevant gas flows in the anode and cathode as shown in Fig. 4. Relations in Fig. 4 consider SOFC reaction with an $\mathrm{O^{=}}$ oxygen ion conducting electrolyte [3]. For both the anode and the cathode, there exists a net inlet flow $\dot{n}_{\mathrm{i},l}$ and a net outlet flow $\dot{n}_{\mathrm{o},l}$, where the subscript 'l' denotes the anode or the cathode. For each reactant, Fig. 4 also shows a flow due to the chemical reactions inside the fuel cell. This flow $\dot{\nu}_{I_{\mathrm{fc}},j}$, where the subscript '$j$' denotes a given reactant, is given as:

$$\dot{\nu}_{I_{\mathrm{fc}},j} = \frac{I_{\mathrm{fc}} N}{z_j F} \tag{20}$$

where z_j is the number of participating electrons per reactant. The values of $z_{\mathrm{H_2}}$, $z_{\mathrm{O_2}}$, and $z_{\mathrm{H_2O}}$ are 2, 4, and 2, respectively. For constant channel pressure at each electrode, molar conservation in the control volume necessitates that the flows $\dot{n}_{\mathrm{i},l}$ and $\dot{n}_{\mathrm{o},l}$ must be balanced by the $\dot{\nu}_{I_{\mathrm{fc}},j}$ flows for each present reactant according to the following equations:

$$\dot{n}_{\mathrm{o,an}} = \dot{n}_{\mathrm{i,an}} - \dot{\nu}_{I_{\mathrm{fc}},\mathrm{H_2}} + \dot{\nu}_{I_{\mathrm{fc}},\mathrm{H_2O}} \tag{21}$$

$$\dot{n}_{\mathrm{o,ca}} = \dot{n}_{\mathrm{i,ca}} - \dot{\nu}_{I_{\mathrm{fc}},\mathrm{O_2}} \tag{22}$$

Additionally, the individual input and output flows in the anode and cathode channels for each reactant are defined as:

$$\dot{\nu}_{\mathrm{i},j} = y_{\mathrm{i},j}\dot{n}_{\mathrm{i},l} \tag{23}$$

$$\dot{\nu}_{\mathrm{o},j} = y_{\mathrm{o},j}\dot{n}_{\mathrm{o},l} \tag{24}$$

where $\dot{\nu}_{\mathrm{i},j}$ is the inlet flow for a given reactant j, and $\dot{\nu}_{\mathrm{o},j}$ is the corresponding outlet flow. The input amount-of-substance fractions $y_{\mathrm{i},j}$ are a property of the gas mixtures being used, and thus are known constants. Under the made assumption of constant channel pressure p_{op}, the output amount-of-substance fractions $y_{\mathrm{o},j}$ are calculated as:

$$y_{\mathrm{o},j} = \frac{p_j^{\mathrm{out}}}{p_{\mathrm{op}}} \tag{25}$$

where p_j^{out} is the partial pressure for a given reactant j at the outlet of the channel. As the partial pressures of the reactants are assumed to change uniformly along the fuel cell tubular channels, the arithmetic mean value can be used to describe the effective partial pressure p_j^{ch} for a given reactant in the anode or cathode channel [2]:

$$p_j^{\mathrm{ch}} = \frac{p_j^{\mathrm{in}} + p_j^{\mathrm{out}}}{2} \tag{26}$$

Using molar conservation, the flows $\dot{\nu}_{\mathrm{i},j}$ and $\dot{\nu}_{\mathrm{o},j}$ for reactant j can be combined with the appropriate $\dot{\nu}_{I_{\mathrm{fc}},j}$ flow to determine the partial pressure p_j^{ch} [16]:

$$\mathrm{H_2 \text{ and } O_2}: \quad \frac{\mathrm{d}p_j^{\mathrm{ch}}}{\mathrm{d}t} = \frac{1}{C_{\mathrm{p},l}}\left(\dot{\nu}_{\mathrm{i},j} - \dot{\nu}_{\mathrm{o},j} - \dot{\nu}_{I_{\mathrm{fc}},j}\right) \tag{27}$$

$$\mathrm{H_2O}: \quad \frac{\mathrm{d}p_j^{\mathrm{ch}}}{\mathrm{d}t} = \frac{1}{C_{\mathrm{p},l}}\left(\dot{\nu}_{\mathrm{i},j} - \dot{\nu}_{\mathrm{o},j} + \dot{\nu}_{I_{\mathrm{fc}},j}\right) \tag{28}$$

where $C_{\mathrm{p},l}$ is the pneumatic capacitance of the fuel cell anode or cathode, and is defined as:

$$C_{\mathrm{p},l} = \frac{V_l}{R \cdot T_{\mathrm{fc}}} \tag{29}$$

where V_l is the volume of the given anode and cathode channel.

B. Implementation

The model for pneumatic transients is implemented in an EMTP-type simulator by representing the anode and cathode using separate equivalent circuits. These circuits are constructed by simultaneously considering one of (21) or (22), depending on the electrode, and one of (27) or (28), depending on the present reactant. For the cathode, this can be accomplished by two electrical nodes linked by transformers, as illustrated in Fig. 5. The implementation for the anode is similar, it can be seen in the complete implementation of the EMTP-type fuel cell model presented in Fig. 9.

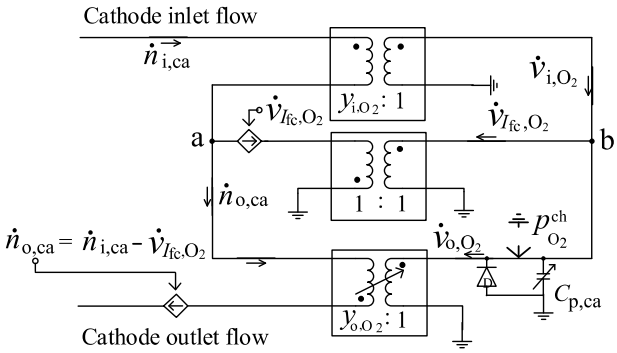

Fig. 5. Implementation of model for pneumatic transients for cathode in PSCAD.

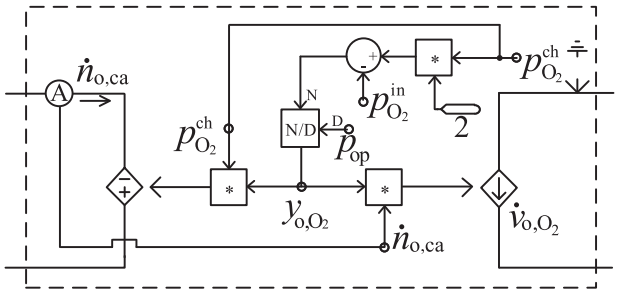

Fig. 6. Variable transformer model used to calculate $y_{\mathrm{o,O_2}}$ in PSCAD.

In Fig. 5, two electrical nodes 'a' and 'b' are linked by three ideal transformers. On the left side of the circuit, three currents meet at the electrical node 'a' in order to model the molar flow-balance in the cathode as given in (22). Inlet flow $\dot{n}_{\mathrm{i,ca}}$ represents the air supply to the cathode. Flows $\dot{\nu}_{I_{\mathrm{fc}},\mathrm{O_2}}$ and $\dot{n}_{\mathrm{o,ca}}$ are modeled as controlled current sources, where $\dot{n}_{\mathrm{o,ca}}$ indicates the outlet flow from the cathode. Current source $\dot{\nu}_{I_{\mathrm{fc}},\mathrm{O_2}}$ is obtained from (20), $\dot{n}_{\mathrm{o,ca}}$ is controlled by an ideal backpressure regulator placed at the outlet of the cathode channel. This control gives a constant pressure in the channel as given by assumption 4 of the Appendix. The controlling signal $\dot{n}_{\mathrm{o,ca}}$ is determined by given $\dot{n}_{\mathrm{i,ca}}$ and $\dot{\nu}_{I_{\mathrm{fc}},\mathrm{O_2}}$ as shown in Fig. 5. Based on (23) and (24), three ideal transformers with the proper turns ratios, as indicated in Fig. 5, are used to transform $\dot{n}_{\mathrm{i,ca}}$, $\dot{\nu}_{I_{\mathrm{fc}},\mathrm{O_2}}$, and $\dot{n}_{\mathrm{o,ca}}$ into $\dot{\nu}_{\mathrm{i,O_2}}$, $\dot{\nu}_{I_{\mathrm{fc}},\mathrm{O_2}}$, and $\dot{\nu}_{\mathrm{o,O_2}}$, respectively. As in (27), the partial pressure of oxygen $p^{\mathrm{ch}}_{\mathrm{O_2}}$ is obtained by calculating the voltage across the capacitance $C_{\mathrm{p,ca}}$ of Fig. 5. The diode prevents negative pressures.

The realization of the variable transformer is depicted in Fig. 6. The variable transformer has a turns ratio of $y_{\mathrm{o,O_2}}$ in order to transform $\dot{n}_{\mathrm{o,ca}}$ into $\dot{\nu}_{\mathrm{o,O_2}}$. The amount-of-substance fraction $y_{\mathrm{o,O_2}}$ of oxygen is a function of the effective partial pressure $p^{\mathrm{ch}}_{\mathrm{O_2}}$ according to (25) and (26), and this variability is indicated in the transformer symbol of Fig. 5. As depicted in Fig. 6, the secondary side connected to the node 'b' of Fig. 5 is modeled through a current-controlled current source $\dot{\nu}_{\mathrm{o,O_2}}$ controlled through the product of $\dot{n}_{\mathrm{o,ca}} \cdot y_{\mathrm{o,O_2}}$. The primary side connected to the node 'a' is modeled through a voltage-controlled voltage source controlled through the product $p^{\mathrm{ch}}_{\mathrm{O_2}} \cdot y_{\mathrm{o,O_2}}$.

TABLE III
ANALOGIES BETWEEN ELECTRICAL AND THERMAL QUANTITIES

Quantity	Electric	Thermal
Potential	Voltage V (V)	Temperature T (K)
Flow	Current I (A)	Heat transfer rate $\dot{Q}$ ($\mathrm{J \cdot s^{-1}}$)
Resistance	Electric resistance R (Ω)	Thermal resistance R_{th} ($\mathrm{K \cdot W^{-1}}$)
Capacitance	Electric capacitance C (F)	Thermal capacitance C_{th} ($\mathrm{J \cdot K^{-1}}$)

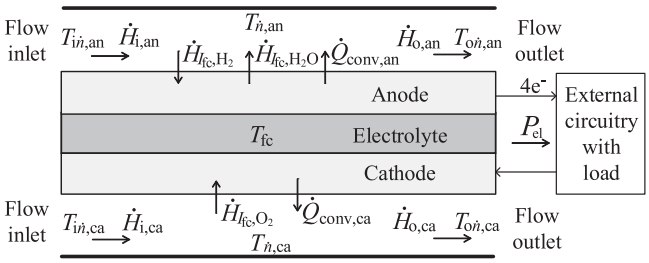

Fig. 7. Fuel cell schematic showing energy flows.

V. MODELING OF THERMAL TRANSIENTS

Due to the temperature dependence of the output voltage, it is important to consider thermal transients when modeling fuel cell behavior in the network. In EMTP-type simulators, this can be accomplished by creating analogies for thermal quantities in the fuel cell stack, as presented in Table III.

A. Mathematical Description

The fuel cell core temperature change varies with the net amount of heat change in the control volume of the solid parts of the stack. The heat change is described by an energy flow balance that includes enthalpy changes due to the chemical reaction, heat transfer to the anode and cathode channels, and the electric power generated [19], [24]:

$$C_{\mathrm{th}}\frac{\mathrm{d}T_{\mathrm{fc}}}{\mathrm{d}t} = \dot{H}_{I_{\mathrm{fc}},\mathrm{H_2}} + \dot{H}_{I_{\mathrm{fc}},\mathrm{O_2}} - \dot{H}_{I_{\mathrm{fc}},\mathrm{H_2O}} - \dot{Q}_{\mathrm{conv,an}} - \dot{Q}_{\mathrm{conv,ca}} - P_{\mathrm{el}} \tag{30}$$

where C_{th} is the thermal capacitance of the fuel cell stack, and the energy flows are defined in Fig. 7.

As shown, $\dot{Q}_{\mathrm{conv},l}$ is a convective heat transfer from fuel cell solid parts to the anode or cathode fluid, $\dot{H}_{I_{\mathrm{fc},j}}$ is the enthalpy flow due to the gas flow of reactant 'j', and P_{el} is the electrical output power of the fuel cell and can be considered as a cooling for the cell. They can be calculated as:

$$\dot{H}_{I_{\mathrm{fc},j}} = \dot{\nu}_{I_{\mathrm{fc},j}} \cdot \overline{h}_j(T_{I_{\mathrm{fc},j}}) \tag{31}$$

$$\dot{Q}_{\mathrm{conv},l} = N k_l A_l (T_{\mathrm{fc}} - T_{\dot{n},l}) \tag{32}$$

$$P_{\mathrm{el}} = V_{\mathrm{fc}} \cdot I_{\mathrm{fc}} \tag{33}$$

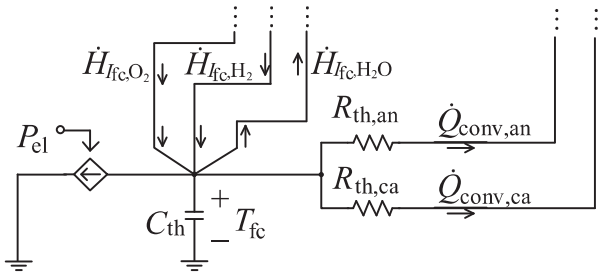

Fig. 8. Implementation of model for thermal transients in PSCAD.

with

$$\overline{h}_j(T_{I_{\mathrm{fc},j}}) = \overline{h}^0_{\mathrm{f},j} + \Delta\overline{h}_j(T_{I_{\mathrm{fc},j}}) = \overline{h}^0_{\mathrm{f},j} + \overline{c}_{\mathrm{p},j}(T_{I_{\mathrm{fc},j}} - T_0) \quad (34)$$

$$T_{\dot{n},l} = \frac{T_{\mathrm{i}\dot{n},l} + T_{\mathrm{o}\dot{n},l}}{2} \quad (35)$$

where $\overline{h}_j(T_{I_{\mathrm{fc},j}})$ is the molar enthalpy of reactant 'j' at temperature $T_{I_{\mathrm{fc},j}}$ [24], it can be obtained by adding the molar enthalpy change $\Delta\overline{h}_j$ between the standard state T_0 and the current state $T_{I_{\mathrm{fc},j}}$ to the enthalpy of formation $\overline{h}^0_{\mathrm{f},j}$ as given in (34), $\overline{c}_{\mathrm{p},j}$ is the molar heat capacity of reactant j, N gives the number of cells, k_l is the convective heat transfer coefficient of the anode fluid or cathode fluid, A_l is the area of the given electrode, $T_{\dot{n},l}$ is the effective temperature of anode fluid or cathode fluid in the tubular channel, it can be presented as an arithmetic mean value as given in (35) [21], T_0 is set to 298.15 K as the standard reference temperature [24], and $T_{I_{\mathrm{fc},j}}$ affiliated with reactant molar flow $\dot{\nu}_{I_{\mathrm{fc},j}}$ can be given as:

$$T_{I_{\mathrm{fc},\mathrm{H_2}}} = T_{\dot{n},\mathrm{an}},\ T_{I_{\mathrm{fc},\mathrm{O_2}}} = T_{\dot{n},\mathrm{ca}},\ T_{I_{\mathrm{fc},\mathrm{H_2O}}} = T_{\mathrm{fc}} \quad (36)$$

The enthalpy flow due to the gas flow at the outlet of the channels is a function of the net outlet flow of fluids discussed in Section IV-A and the outlet temperatures [19], [24]:

$$\dot{H}_{\mathrm{o,an}} = \dot{n}_{\mathrm{o,an}} \cdot \overline{h}_{\mathrm{o,an}}(T_{\mathrm{o}\dot{n},\mathrm{an}}) \quad (37)$$

$$\dot{H}_{\mathrm{o,ca}} = \dot{n}_{\mathrm{o,ca}} \cdot \overline{h}_{\mathrm{o,ca}}(T_{\mathrm{o}\dot{n},\mathrm{ca}}) \quad (38)$$

To calculate the fluid output temperatures $T_{\mathrm{o}\dot{n},l}$, the energy balances of Fig. 7 are considered [19], [24]:

$$\dot{H}_{\mathrm{o,an}} = \dot{H}_{\mathrm{i,an}} + \dot{Q}_{\mathrm{conv,an}} + \dot{H}_{I_{\mathrm{fc},\mathrm{H_2O}}} - \dot{H}_{I_{\mathrm{fc},\mathrm{H_2}}} \quad (39)$$

$$\dot{H}_{\mathrm{o,ca}} = \dot{H}_{\mathrm{i,ca}} + \dot{Q}_{\mathrm{conv,ca}} - \dot{H}_{I_{\mathrm{fc},\mathrm{O_2}}} \quad (40)$$

The incoming flows and input temperatures are known. Inserting (31) to (38) into (39) and (40), the fluid outlet temperatures $T_{\mathrm{o}\dot{n},l}$ can then be found. Those temperatures $T_{\mathrm{o}\dot{n},\mathrm{an}}$ and $T_{\mathrm{o}\dot{n},\mathrm{ca}}$ are needed to calculate the fuel cell temperature T_{fc} in (30).

B. Implementation

The equations describing the thermal transients in an SOFC can be represented in an EMTP-type simulator using the equivalent circuit model presented in Fig. 8. To facilitate circuit modeling, several parameters in (32) are lumped into thermal resistances: $R_{\mathrm{th},l} = 1/(Nk_lA_l)$. The capacitive branch consists of a capacitance C_{th}, and the resistive branches comprise two parallel resistances $R_{\mathrm{th,an}}$ and $R_{\mathrm{th,ca}}$. The controlling signal for the dependent current source is P_{el}, which is determined by (33). To model (30), P_{el} is connected as shown in Fig. 8. Each of the two thermal resistances will connect to a voltage source characterizing either the effective temperature of the anode or cathode fluid in the electrode channels as shown in Fig. 9 of the complete connections. The currents $\dot{H}_{I_{\mathrm{fc},\mathrm{O_2}}}$, $\dot{H}_{I_{\mathrm{fc},\mathrm{H_2}}}$, and $\dot{H}_{I_{\mathrm{fc},\mathrm{H_2O}}}$ flowing through the three branches marked by the dots represent the enthalpy flows carried by the chemical reactants. Complete connections of these three branches are depicted in the model for thermal transients of Fig. 9. The enthalpy flow for each present reactant $\dot{H}_{I_{\mathrm{fc},j}}$ is implemented using a current-controlled current source. The controlling signal is determined by (31) as shown in the upper left part of Fig. 9, where the circuit implementation of energy balances of anode and cathode fluids is presented. Finally, according to (30), the fuel cell temperature T_{fc} is obtained by calculating the voltage across the capacitance C_{th} as shown in Fig. 8.

TABLE IV
OPERATING POINT PARAMETERS FOR VALIDATION

Operating point parameters for 3 W SOFC					
$y_{\mathrm{i,H_2}}$	0.9	$\dot{n}_{\mathrm{i,an}}$ (mol/s)	7.39×10^{-5}	$T_{\mathrm{i}\dot{n},l}$ (K)	1023
$y_{\mathrm{i,O_2}}$	0.21	$\dot{n}_{\mathrm{i,ca}}$ (mol/s)	1.07×10^{-3}	p_{op} (Pa)	101325
Operating point parameters for 5 kW SOFC					
$y_{\mathrm{i,H_2}}$	0.9	$\dot{n}_{\mathrm{i,an}}$ (mol/s)	0.096	$T_{\mathrm{i}\dot{n},l}$ (K)	1173
$y_{\mathrm{i,O_2}}$	0.21	$\dot{n}_{\mathrm{i,ca}}$ (mol/s)	1.234	p_{op} (Pa)	303975

VI. INTEGRATION OF ELECTRIC, PNEUMATIC, AND THERMAL TRANSIENTS

For the complete fuel cell, all diverse transients are simulated simultaneously. The circuit implementation in PSCAD is shown in Fig. 9. The organization of Fig. 9 corresponds to the concept of Fig. 1.

In Fig. 9, the model for electric transients described in Section III is located in the lower right part. The model for thermal transients is located on the left. This model was described in Section V. The energy balances of anode and cathode fluids described by (39) and (40), respectively, are implemented in the upper left part. For the model of pneumatic transients, the equivalent circuit of the cathode, as depicted in Fig. 5, is located in the upper right corner of the diagram. The equivalent circuit used to model pneumatic transients in the anode is shown in the middle part on the right. It is similar in structure to the circuit shown in Fig. 5. The upper double-tap transformer has turns ratios of $y_{\mathrm{i,H_2}}$ and $y_{\mathrm{i,H_2O}}$ in order to model (23). Similarly, the double-tap variable transformer has turns ratios of $y_{\mathrm{o,H_2}}$ and $y_{\mathrm{o,H_2O}}$ in order to model (24), and it is similar to the variable transformer shown in Fig. 6. Flows $\dot{\nu}_{I_{\mathrm{fc},\mathrm{H_2}}}$ and $\dot{\nu}_{I_{\mathrm{fc},\mathrm{H_2O}}}$ required by (27) and (28) are modeled as two controlled current sources using (20). The partial pressures $p^{\mathrm{ch}}_{\mathrm{H_2}}$ and $p^{\mathrm{ch}}_{\mathrm{H_2O}}$ are obtained using equivalent circuit presentations of (27).

Thanks to the modular approach followed, Fig. 1 also offers insight into the opportunity to reduce the SOFC model if only

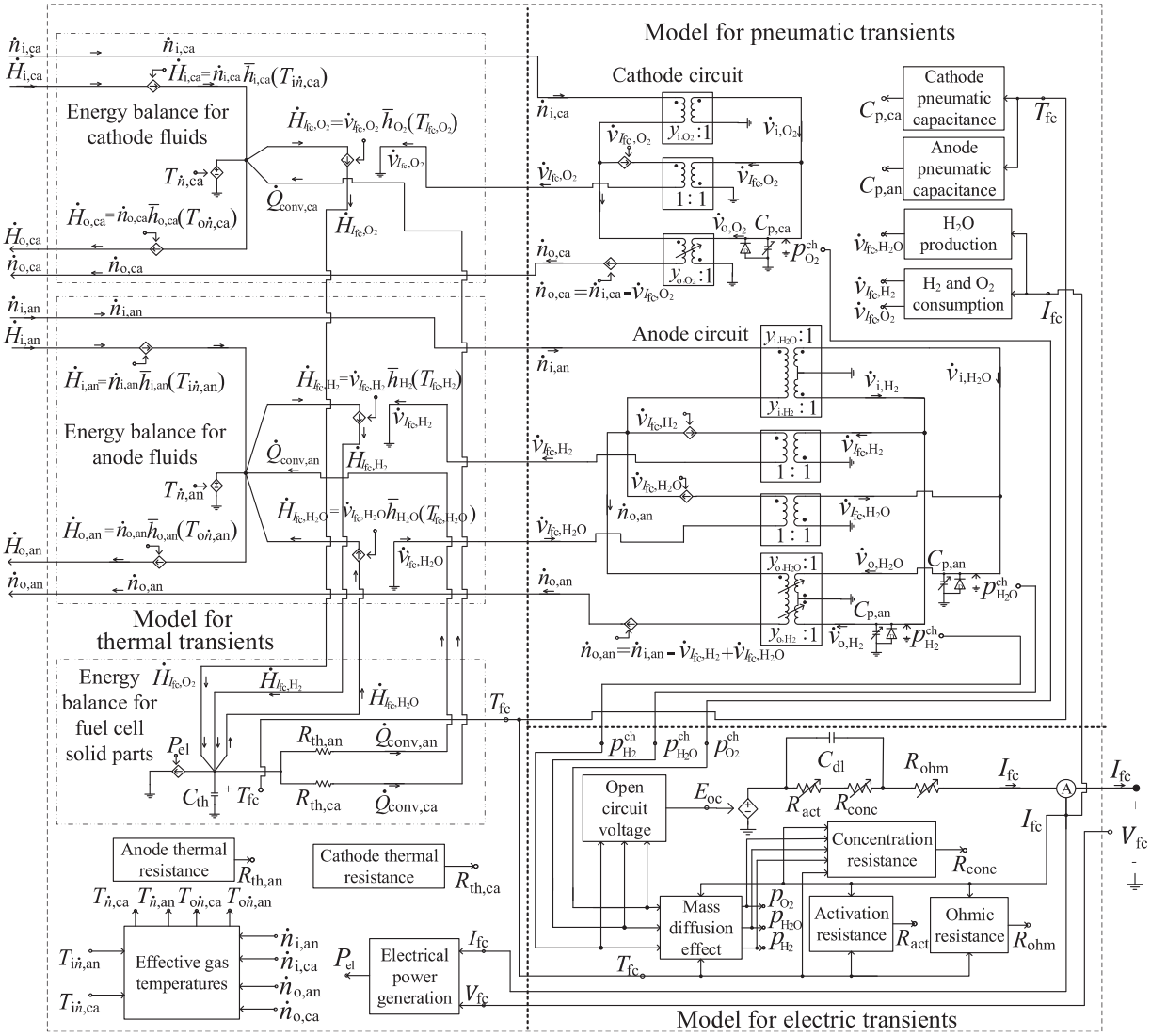

Fig. 9. Implementation of models for electric, pneumatic, and thermal transients in PSCAD.

a reduced set of transients is of interest. For example, if only electric transients are of interest, then the respective blocks in Fig. 1 and Fig. 9 called "Model for electric transients" can be used as a dedicated SOFC model. The interface variables $T_{\rm fc}$, $p^{\rm ch}_{\rm H_2}$, $p^{\rm ch}_{\rm O_2}$, and $p^{\rm ch}_{\rm H_2O}$ are then set as inputs by the user.

VII. Validation

The modeling is validated for steady state and transients of different scales. Two instantiations of the SOFC in PSCAD shown in Fig. 9 with operating point parameters in Table IV are considered. One instantiation is a 3 W micro-tubular SOFC, and the other is a 5 kW tubular SOFC. The fuel cell parameters shown in Table V of the Appendix are adapted based on [3], [16], [21], [25] and [26]. With these two parameter sets, the fuel cell models can respectively represent the behaviors of the 3 W micro-tubular SOFC stack reported in [26] and the 5 kW tubular SOFC stack reported in [21]. Some of the parameters, such as for the double layer capacitance, can be obtained by using AC impedance spectroscopy techniques [27].

The 3 W micro-tubular SOFC stack comprises six cells connected in series. For the purpose of validation, the reference data of this SOFC stack, including the polarization curve characteristics and the fast transient responses, were compiled from the experimental data reported in [26]. The corresponding experimental setup was also described in [26]. The 5 kW tubular SOFC stack comprises 96 cells connected in series. The reference data of this fuel cell stack, including polarization curve characteristics and the slow transient responses, were compiled from the results reported in [21]. With the help of these two fuel cell stacks, the modeling can be validated for steady state, fast transients, and slow transients.

A. Polarization Curve Validation

Both the 3 W SOFC model and the 5 kW SOFC model are used for validating the steady state behavior. The validation results of the polarization curve characteristics of the 3 W SOFC are given in Fig. 10. The operating temperature of the fuel cell model is maintained at 1023 K according to assumption 9 in the

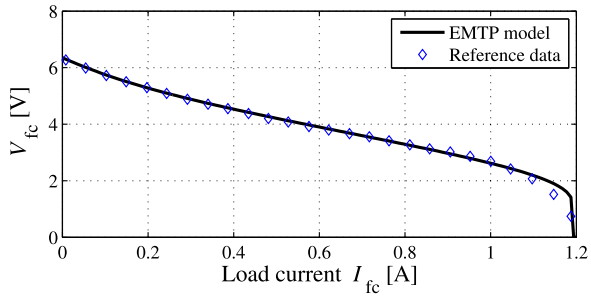

Fig. 10. Model polarization curve compared with reference data of 3 W SOFC.

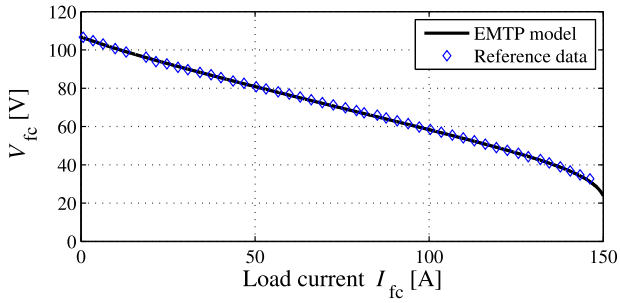

Fig. 11. Model polarization curve compared with reference data of 5 kW SOFC.

Appendix. The results show matching simulation and reference data in all regions: region of low currents, where activation losses dominate; middle region, where ohmic losses dominate and where the voltage drop is proportional to the current; and region of high currents, where the voltage drops towards zero due to the low partial pressures of reactants. Fig. 11 shows the validation results of the polarization curve characteristics of the 5 kW SOFC. The operating temperature is 1173 K. Here, simulation and reference data match in all regions as well.

B. Fast Transients

The electric transient due to the double layer capacitance is the fastest transient in the fuel cell, occurring on the order of tens of milliseconds. This transient is validated by comparing the simulation results of the 3 W micro-tubular SOFC with the corresponding reference data reported in [26]. The validation is based on the simulation of a load current step. The fuel cell load current is at 0.1 A until time 30 s, at which point the fuel cell load current steps up to 0.8 A. The resulting voltage transient can be seen in Fig. 12. The transient profile shows a voltage step due to an instantaneous decrease in ohmic losses, followed by a first order response governed by the double layer capacitance. Both these stages of the fast transient are visible in the simulation and the experiment.

C. Slow Transients

The thermal transient is the slowest in the SOFC, with a time constant in the tens of minutes. To validate the slow transient behavior of the SOFC model, the 5 kW SOFC model is simulated, and the results are compared with the reference data presented in [21]. The test simulation used for comparison begins with the fuel cell in steady state at a load current of 100 A. The load

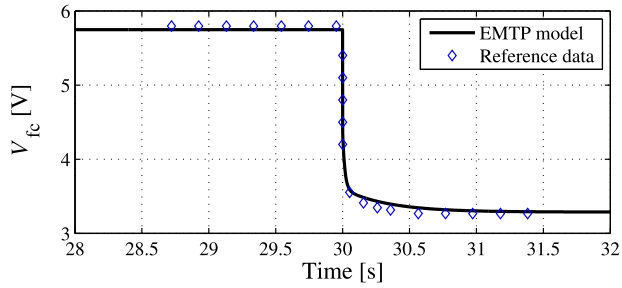

Fig. 12. Model response to load transients at small time scale and comparison with reference data of 3 W SOFC.

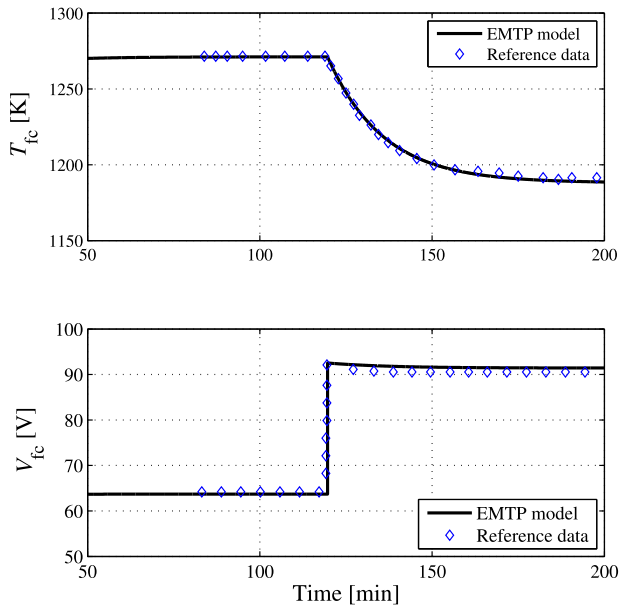

Fig. 13. Model response to load transients at large time scale and comparison with reference data of 5 kW SOFC.

current steps to 30 A after 120 minutes. The resulting fuel cell voltage response is shown in Fig. 13. The voltage curve first rises above its steady state value when encountering the current change. After reaching the peak, it then gradually recovers back to the final value in several tens of minutes due to the thermal transient of the fuel cell. The fuel cell voltage decreases with fuel cell temperature primarily because the ohmic resistance $R_{\rm ohm}$ defined in (10) increases with decreasing fuel cell temperature. As for the polarization curve and the fast transient, the simulation of the slow transient also closely matches the reference.

VIII. Application: Multiphysics Load-Following Transients of CHP Plant

The SOFC is characterized by high operating temperature, which makes the hot exhaust streams more valuable. The SOFC-based CHP can produce electricity while utilizing the generated heat that would be wasted otherwise [3], [4]. In this section, the 5 kW SOFC model validated in Section VII is used in a CHP application study. To sustain the electrochemical reactions within the SOFC, it is important to maintain the fuel cell temperature at a proper level [3]. When the SOFC is connected to a load

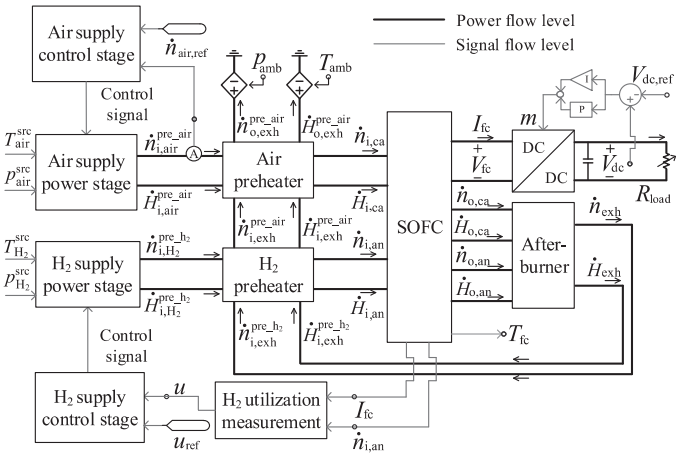

Fig. 14. Implementation of application case in PSCAD.

and starts to generate electric power, the inlet fluids, including the air and hydrogen, are preheated by using the SOFC exhaust streams.

The implementation of such a thermally self-sustaining CHP system is shown Fig. 14. The system comprises an SOFC stack, an afterburner, two preheaters, a hydrogen supply system, and an air supply system [3], [28]. It is noted that for any fluid flow, the molar flow rate and the enthalpy flow appear as a pair. The block "SOFC" represents the model of Fig. 9. A hydrogen supply system and an air supply system feed reactants to the fuel cell anode and cathode, respectively. The exhaust fluids of the SOFC consist of nitrogen and oxygen from the cathode and unused hydrogen and produced water vapor from the anode. All these fluids go into the afterburner to further elevate the fluid temperature. In the two preheaters, the exhaust heat is harnessed and used for preheating the inlet hydrogen and air flows. Modeling details of these components are given in Appendix XII. Parameters are listed in Tables VI and VII of Appendix XI. The "H_2 utilization measurement" block located in the lower part of Fig. 14 calculates the hydrogen utilization. Hydrogen utilization is an important control parameter for fuel cell operation and will be used for hydrogen flow control. It can be calculated as follows:

$$u = \frac{\dot{\nu}_{I_{\mathrm{fc}},\mathrm{H}_2}}{\dot{\nu}_{\mathrm{i,H}_2}} = \frac{NI_{\mathrm{fc}}}{2F\dot{n}_{\mathrm{i,an}}y_{\mathrm{i,H}_2}} \tag{41}$$

The setup in Fig. 14 illustrates how the implemented multiphysics fuel cell system is interfaced with other electric, pneumatic, and thermal circuitry. It is critical to have the fuel flowing in the pneumatic circuit to be adjusted in accordance with the load. For example, the "H_2 supply control stage" acts on the "H_2 supply power stage" to adapt the supply. Furthermore, it is desirable to control the load voltage through power electronic conversion [2]. The following application case also illustrates how different controls and transients interact.

A. Electric and Pneumatic Load-Following Transient

As indicated in Fig. 14, a boost converter keeps the load voltage to a desired level V_{dc}. Changes in load $P_{\mathrm{load,ref}}$ are

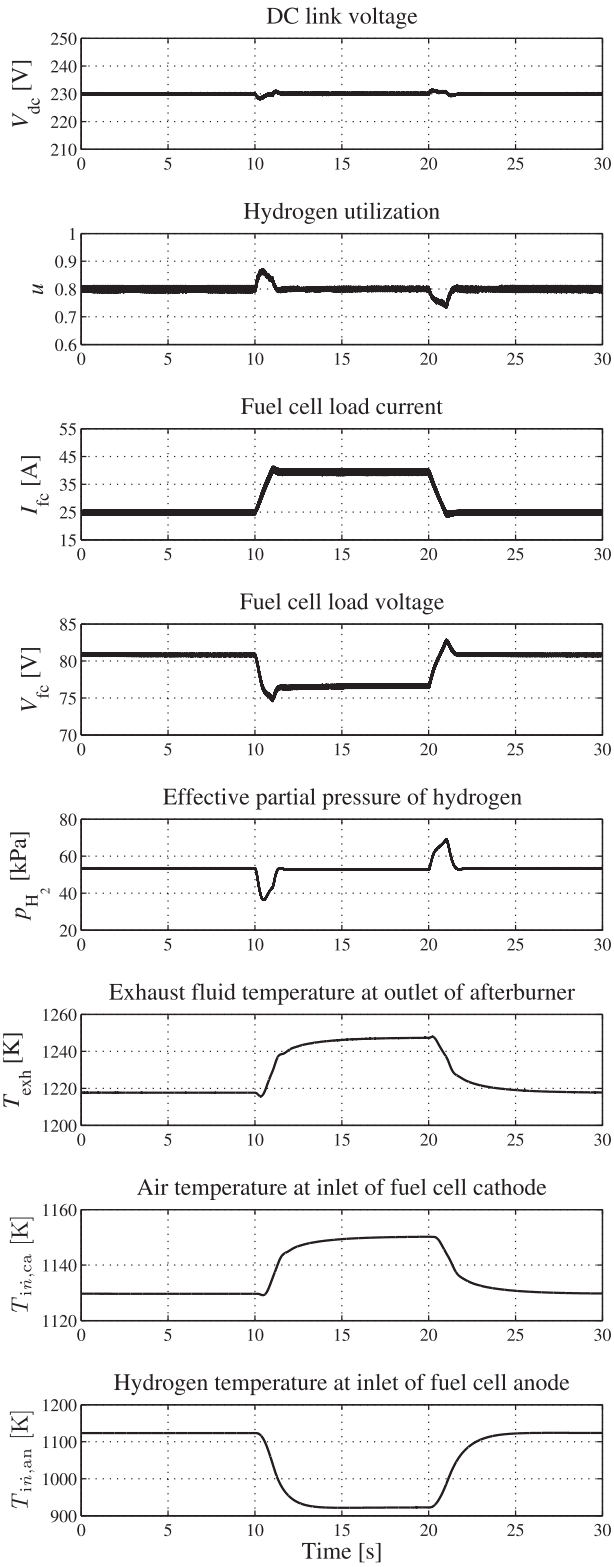

Fig. 15. Simulation of multiphysics load-following transients of CHP plant.

simulated by modifying the variable resistance according to $R_{\mathrm{load}} = V_{\mathrm{dc,ref}}^2/P_{\mathrm{load,ref}}$. In order to avoid fuel starvation, the power supplied by the fuel cell is limited to a certain maximum rate [29], [30]. The responses of diverse quantities to load changes are shown in Fig. 15. The fuel cell system initially is in steady state supplying a load of 2000 W. At time 10 s, the

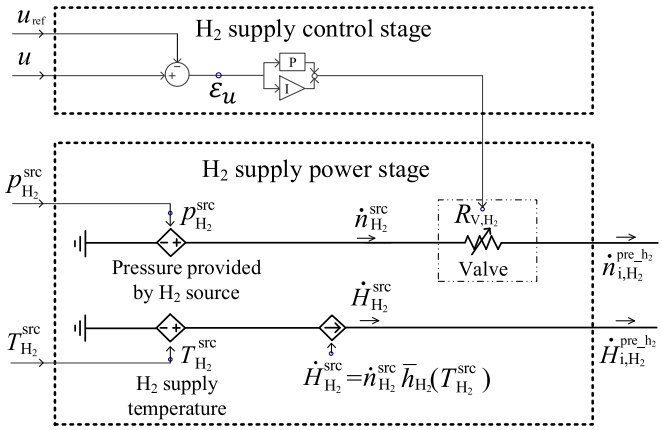

Fig. 16. Implementation of H_2 supply system with control in PSCAD.

reference load profile $P_{\mathrm{load,ref}}$ increases to 3000 W at a rate of 1000 $\mathrm{W/s}$. At time 20 s, $P_{\mathrm{load,ref}}$ decreases at that rate to a final value of 2000 W. The DC bus voltage V_{dc} is maintained at 230 V as shown in the first column of Fig. 15. The maximum deviation during the transients is less than 5 V. The responses of the hydrogen utilization are also presented in Fig. 15. The results show that u is kept between 0.7 and 0.9 during the transients. The applied hydrogen flow control is given in Appendix XII-A. Fig. 15 also shows the simulation results for I_{fc}, V_{fc}, and $p_{\mathrm{H_2}}$. Quantities I_{fc} and V_{fc} represent the involved electric transients of the fuel cell and show the ripples of the 10 kHz switching of the boost converter. The partial pressure $p_{\mathrm{H_2}}$ is of interest for studies concerning fuel cell durability [31].

B. Thermal Load-Following Transient

In the two preheaters, heat is transferred from the exhaust fluid of the afterburner to the fuel cell inlet flows. Quantity T_{exh} shown in Fig. 15 is the temperature of the exhaust fluid at the outlet of the afterburner. Quantities $T_{\mathrm{i}\dot{n},\mathrm{ca}}$ and $T_{\mathrm{i}\dot{n},\mathrm{an}}$ are the temperatures of the fluids at the inlets of the fuel cell cathode and anode, respectively. These temperature curves represent the thermal transients of the CHP system. As an example, at time 10 s, the temperature at the outlet of the afterburner T_{exh} first drops lower at the load increment and then gradually increases to a steady state value. This behavior can be explained as follows. Since the hydrogen consumption rises proportionally to the fast-changing current I_{fc} according to (20), the hydrogen utilization ratio u also rises initially. A larger u indicates that less unused hydrogen is fed to the afterburner. Thus, an initial drop in T_{exh} is observed. As the hydrogen utilization is brought back to 0.8 by means of the action of the hydrogen supply control stage of Fig. 16, more unused hydrogen is fed to the afterburner, resulting in the rise in T_{exh}.

As expected, the air temperature $T_{\mathrm{i}\dot{n},\mathrm{ca}}$ rises with the exhaust fluid temperature T_{exh}. But even though T_{exh} rises, the hydrogen temperature $T_{\mathrm{i}\dot{n},\mathrm{an}}$ drops with the control implemented. This is because the electric load increase trigged an increase in hydrogen flow drawn from a source at 298 K. The above observation and discussion show the close interactions of multi-physics transients in an SOFC-CHP application. The results illustrate the insight gained by representing electric, pneumatic, and thermal circuits simultaneously.

IX. Conclusion

A methodology for simulating multi-physics transients in EMTP-type network simulators was developed, implemented, validated, and applied to the modeling of a solid oxide fuel cell. The presented work is distinguished through three scientific contributions. First, the modeling of mutually coupled electric, pneumatic, and thermal circuits was formulated. Second, it was shown how the method can be applied in the modeling of an SOFC in EMTP-type simulation using circuit elements from standard libraries of PSCAD. Third, the performed validation shows a close matching of simulation and reference data for the steady state and diverse transients. In a comprehensive combined heat and power application study, the model computed multi-physics transients at a level of insight that has not been reached so far by power network simulators.

X. Appendix: Assumptions

To facilitate the modeling of the multi-physics SOFC, the following assumptions are made:

1) Parameters for single fuel cells can be aggregated to model an entire fuel cell stack with further electromechanical assistance.
2) The model is one-dimensional in the direction of the electrolyte. A two-dimensional extension along the channel would involve multiple control volumes as in Figs. 4 and 7.
3) All reactant gases are perfect gases. Based on this assumption, the ideal gas law stands, and (27) and (28) can then be established [24].
4) Total pressures in the fuel cell gas flow channels are assumed to be constant.
5) The gases are assumed to be preheated before flowing into the fuel cell stack.
6) During normal fuel cell operation, the fuel cell is at thermal equilibrium, and heat generated in the fuel cell is balanced with the anode and cathode fluids [19].
7) It is assumed that the temperature is uniformly distributed in the solid parts so that the radiation between solid parts is not taken into account. Moreover, radiation heat transfer between the solid parts and the fluids is neglected compared with the convective heat transfer [32].
8) To shorten start-up of the simulation, the SOFC stack should be in hot standby mode [33], [34]. Based on this assumption, the SOFC stack can avoid the heat-up process and directly start to operate when it is connected to a load.
9) For the validation of the polarization curve of the model, it is assumed that the fuel cell operating temperature is maintained [21], [26].
10) The afterburner and the two preheaters used in the application are assumed to be lossless.

XI. Appendix: Validation and Application Case Parameters

TABLE V
FUEL CELL PARAMETERS

Parameters for 3 W SOFC			
$W_{\rm act}$ (kJ/mol)	120	α	0.63
B (kA)	90.50	δ (K)	-3722
$C_{\rm dl}$ (F)	1.27×10^{-2}	ξ_0 (V)	0.14
$C_{\rm th}$ (J/K)	0.28	ξ_1 (V/K)	-3.43×10^{-5}
$k_{\rm an}$ (W/(m$^2\cdot$K))	33.85	γ (Ω)	0.28
$k_{\rm ca}$ (W/(m$^2\cdot$K))	50.06	T_γ (K)	973
N	6	$k_{\rm E}$ (V/K)	1.78×10^{-4}
Parameters for 5 kW SOFC			
$W_{\rm act}$ (kJ/mol)	114	α	0.22
B (kA)	1.38×10^{4}	δ (K)	-3757
$C_{\rm dl}$ (F)	0.04	ξ_0 (V)	0.12
$C_{\rm th}$ (J/K)	5.54×10^{4}	ξ_1 (V/K)	-3.10×10^{-5}
$k_{\rm an}$ (W/(m$^2\cdot$K))	22.39	γ (Ω)	4.87×10^{-3}
$k_{\rm ca}$ (W/(m$^2\cdot$K))	52.58	T_γ (K)	973
N	96	$k_{\rm E}$ (V/K)	1.47×10^{-4}

TABLE VI
BOOST CONVERTER PARAMETERS

Quantity	Value
Switching frequency	10 kHz
DC bus voltage	230 V
DC bus capacitance	2000 μF
Converter side inductance	5 mH

TABLE VII
CHP PARAMETERS

$u_{\rm ref}$	0.8	$\dot{n}_{\rm air,ref}$ (mol/s)	1.234
$p_{\rm amb}$ (Pa)	101325	$T_{\rm amb}$ (K)	298
$p_{\rm H_2}^{\rm src}$ (Pa)	$10p_{\rm amb}$	$T_{\rm H_2}^{\rm src}$ (K)	298
$p_{\rm op}$ (Pa)	303975	T_0 (K)	298
$p_{\rm o,air}^{\rm comp}$ (Pa)	$1.2p_{\rm op}$	$T_{\rm i,air}^{\rm comp}$ (K)	298
φ	1.4	$\eta_{\rm c}$	0.76
$\overline{h}^0_{\rm f,H_2}$ (kJ/mol)	0	$\overline{h}^0_{\rm f,O_2}$ (kJ/mol)	0
$\overline{h}^0_{\rm f,N_2}$ (kJ/mol)	0	$\overline{h}^0_{\rm f,H_2O}$ (kJ/mol)	-241.82
$\overline{c}_{\rm p,H_2}$ (J/(mol$\cdot$K))	29.5	$\overline{c}_{\rm p,O_2}$ (J/(mol$\cdot$K))	33.4
$\overline{c}_{\rm p,N_2}$ (J/(mol$\cdot$K))	31.1	$\overline{c}_{\rm p,H_2O}$ (J/(mol$\cdot$K))	38.1

XII. Appendix: Modeling and Implementation of CHP Components

In this section, supplementary information on the application of Fig. 14 is given.

A. Hydrogen Supply System

A pressure source, which represents a store, drives the hydrogen inlet flow through the controlling valve in Fig. 16. The enthalpy flow due to this hydrogen flow is calculated by:

$$\dot{H}_{\rm H_2}^{\rm src} = \dot{n}_{\rm H_2}^{\rm src}\cdot\overline{h}_{\rm H_2}(T_{\rm H_2}^{\rm src}) \tag{42}$$

where 'src' stands for source.

For SOFC operation, it is necessary to design a controller which maintains a range for the hydrogen utilization ratio u between 0.7 and 0.9 [30]. This can be accomplished by using a proportional integral (PI) controller to regulate the inlet flow to the anode $\dot{n}_{\rm i,an}$ since (41) shows $\dot{n}_{\rm i,an}$ to be proportional to $I_{\rm fc}$ for a given u. The input error signal ε_u to the PI controller is calculated as follows:

$$\varepsilon_u = (u - u_{\rm ref}) \tag{43}$$

where $u_{\rm ref}$ is the desired reference hydrogen utilization.

As shown in Fig. 14, the measurements taken from the module SOFC provide the value of the hydrogen utilization u to be compared with its reference $u_{\rm ref}$. The upper circuit of the hydrogen power supply stage in Fig. 16 is used for representing the hydrogen flow, while the lower circuit represents the affiliated enthalpy flow. Regarding the hydrogen flow circuit, the pressure is modeled according to the pressure-voltage analogy. The valve is modeled as a variable resistance. It is regulated by the PI controller. The enthalpy flow $\dot{H}_{\rm H_2}^{\rm src}$ due to the molar flow $\dot{n}_{\rm H_2}^{\rm src}$ is implemented using a current controlled current source, whose controlling signal is $\dot{n}_{\rm H_2}^{\rm src}\cdot\overline{h}_{\rm H_2}(T_{\rm H_2}^{\rm src})$ according to (42). The voltage source with the controlling signal of $T_{\rm H_2}^{\rm src}$ indicates the supply temperature of the hydrogen.

B. Air Supply System

The air supply system may be modeled in a similar way as the hydrogen supply system. If a compressor is involved for providing the force for driving the air, then this should be accounted for in the model. The air flow rate can still be regulated by a valve as in Fig. 16.

The enthalpy flow of the air flow at the outlet of the compressor is calculated by:

$$\dot{H}_{\rm o,air}^{\rm comp} = \dot{H}_{\rm i,air}^{\rm comp} + \Delta\dot{H}_{\rm air}^{\rm comp} \tag{44}$$

with

$$\dot{H}_{\rm i,air}^{\rm comp} = \dot{n}_{\rm i,air}^{\rm comp}\cdot\overline{h}_{\rm air}(T_{\rm i,air}^{\rm comp}) \tag{45}$$

$$\Delta\dot{H}_{\rm air}^{\rm comp} = \dot{n}_{\rm i,air}^{\rm comp}\cdot\overline{c}_{\rm p,air}\cdot(T_{\rm o,air}^{\rm comp} - T_{\rm i,air}^{\rm comp}) \tag{46}$$

where $\dot{H}_{\rm i,air}^{\rm comp}$ is the enthalpy flow of the air flow at the inlet of the compressor, $\Delta\dot{H}_{\rm air}^{\rm comp}$ is the enthalpy increment of the air flow due to the compression, and $T_{\rm o,air}^{\rm comp}$ is the compressor outlet temperature of the air.

The temperature of the air at the outlet of the compressor $T_{\rm o,air}^{\rm comp}$ is given as [3]:

$$T_{\rm o,air}^{\rm comp} = T_{\rm i,air}^{\rm comp} + \frac{T_{\rm i,air}^{\rm comp}}{\eta_{\rm c}}\left(\left(\frac{p_{\rm o,air}^{\rm comp}}{p_{\rm i,air}^{\rm comp}}\right)^{\frac{\varphi-1}{\varphi}} - 1\right) \tag{47}$$

where $T_{\rm i,air}^{\rm comp}$ is the temperature of the air at the inlet of the compressor, φ is the ratio of the heat capacities of the air, $\eta_{\rm c}$ is the isentropic efficiency of the compressor, $p_{\rm i,air}^{\rm comp}$ and $p_{\rm o,air}^{\rm comp}$ are the air pressures at the inlet and outlet of the compressor, respectively.

C. Afterburner

In the SOFC, the hydrogen utilization is maintained between 0.7 and 0.9 [30]. The unused hydrogen in $\dot{n}_{\mathrm{o,an}}$ is combusted in a burner according to the following reaction:

$$\mathrm{H_2} + \frac{1}{2}\mathrm{O_2} \rightarrow \mathrm{H_2O}\,, \tag{48}$$

The molar conservation necessitates that the inlet flows $\dot{n}_{\mathrm{o},l}$, which are also the outlet flows from the SOFC as discussed in Table I, and the afterburner outlet flow $\dot{n}_{\mathrm{exh}}$ must be balanced by the flows for each present reactant according to the following equation:

$$\dot{n}_{\mathrm{exh}} = \dot{n}_{\mathrm{o,an}} + \dot{n}_{\mathrm{o,ca}} - \dot{\nu}_{\mathrm{H_2}} - \dot{\nu}_{\mathrm{O_2}} + \dot{\nu}_{\mathrm{H_2O}} \tag{49}$$

where the subscript 'exh' stands for exhaust, $\dot{\nu}_{\mathrm{H_2}}$, $\dot{\nu}_{\mathrm{O_2}}$, and $\dot{\nu}_{\mathrm{H_2O}}$ are the molar flow rates of the reactants in the afterburner for $\mathrm{H_2}$, $\mathrm{O_2}$, and $\mathrm{H_2O}$, respectively. It is assumed that the unused hydrogen is completely combusted in the afterburner. Flow $\dot{\nu}_{\mathrm{H_2}}$ is therefore given as:

$$\begin{aligned}\dot{\nu}_{\mathrm{H_2}} &= \dot{\nu}_{\mathrm{o,H_2}} \\ &= y_{\mathrm{o,H_2}}\dot{n}_{\mathrm{o,H_2}}\end{aligned} \tag{50}$$

where $\dot{\nu}_{\mathrm{o,H_2}}$ is the unused hydrogen in the anode fluid from the fuel cell as defined in (24). Based on the chemical reaction of (48), $\dot{\nu}_{\mathrm{O_2}}$ and $\dot{\nu}_{\mathrm{H_2O}}$ can be obtained from $\dot{\nu}_{\mathrm{H_2}}$:

$$\dot{\nu}_{\mathrm{O_2}} = \frac{1}{2}\dot{\nu}_{\mathrm{H_2}} \tag{51}$$

$$\dot{\nu}_{\mathrm{H_2O}} = \dot{\nu}_{\mathrm{H_2}} \tag{52}$$

In order to obtain the energy flow at the outlet of the afterburner, the following energy balance for the afterburner is established [24]:

$$\dot{H}_{\mathrm{o,an}} + \dot{H}_{\mathrm{o,ca}} = \dot{H}_{\mathrm{exh}} \tag{53}$$

and

$$\begin{aligned}\dot{H}_{\mathrm{exh}} &= \dot{n}_{\mathrm{exh}} \cdot \overline{h}_{\mathrm{exh}}(T_{\mathrm{exh}}) \\ &= \dot{n}_{\mathrm{exh}} \cdot \left(\overline{h}^{0}_{\mathrm{f,exh}} + \overline{c}_{\mathrm{p,exh}}(T_{\mathrm{exh}} - T_0)\right)\end{aligned} \tag{54}$$

where $\overline{h}^{0}_{\mathrm{f,exh}}$ is the enthalpy of formation of the exhaust fluid, and $\overline{c}_{\mathrm{p,exh}}$ is the molar heat capacity of the exhaust fluid. They can be calculated by [24]:

$$\overline{h}^{0}_{\mathrm{f,exh}} = \sum_{i=1}^{Z} y_i \overline{h}^{0}_{\mathrm{f},i},\ \overline{c}_{\mathrm{p,exh}} = \sum_{i=1}^{Z} y_i \overline{c}_{\mathrm{p},i} \tag{55}$$

where $\overline{h}^{0}_{\mathrm{f},i}$ and $\overline{c}_{\mathrm{p},i}$ respectively are the enthalpy of formation and molar heat capacity of constituent i, y_i is the amount-of-substance fraction of constituent i, and Z is the total number of the constituents in the fluid.

According to (54), the temperature of the exhaust fluid at the outlet of the afterburner T_{exh} can be determined based on $\dot{n}_{\mathrm{exh}}$ and $\dot{H}_{\mathrm{exh}}$.

D. Preheaters

The two preheaters can be modeled based on the molar conservation and energy balance [24], [33]. In the following, the model for the hydrogen preheater is given. The air preheater can be modeled in a similar way.

For the hydrogen preheater of Fig. 14, the following molar conservation can be established for the inlet and outlet flows:

$$\dot{n}_{\mathrm{i,an}} = \dot{n}^{\mathrm{pre\_h_2}}_{\mathrm{i,H_2}} \tag{56}$$

$$\dot{n}^{\mathrm{pre\_h_2}}_{\mathrm{o,exh}} = \dot{n}^{\mathrm{pre\_h_2}}_{\mathrm{i,exh}} \tag{57}$$

where $\dot{n}^{\mathrm{pre\_h_2}}_{\mathrm{o,exh}} = \dot{n}^{\mathrm{pre\_air}}_{\mathrm{i,exh}}$ in Fig. 14.

The thermal power is transferred from the hot fluid to the cold fluid. It is assumed that the preheater is lossless, the energy decrement in the hot fluid thus equals the energy increment in the cold fluid:

$$\Delta\dot{Q}^{\mathrm{pre\_h_2}}_{\mathrm{exh}} = \dot{H}^{\mathrm{pre\_h_2}}_{\mathrm{i,exh}} - \dot{H}^{\mathrm{pre\_h_2}}_{\mathrm{o,exh}} \tag{58}$$

$$\Delta\dot{Q}^{\mathrm{pre\_h_2}}_{\mathrm{exh}} = \dot{H}^{\mathrm{pre\_h_2}}_{\mathrm{o,H_2}} - \dot{H}^{\mathrm{pre\_h_2}}_{\mathrm{i,H_2}} \tag{59}$$

where the superscript 'pre_$\mathrm{h_2}$' stands for $\mathrm{H_2}$ preheater, $\Delta\dot{Q}^{\mathrm{pre\_h_2}}_{\mathrm{exh}}$ is the heat exchanged between the hot and cold fluids. Combining (58) and (59), the enthalpy flow affiliated with the exhaust fluid coming out of the fuel preheater $\dot{H}^{\mathrm{pre\_h_2}}_{\mathrm{o,exh}}$ is determined by:

$$\dot{H}^{\mathrm{pre\_h_2}}_{\mathrm{o,exh}} = \dot{H}^{\mathrm{pre\_h_2}}_{\mathrm{i,exh}} - (\dot{H}^{\mathrm{pre\_h_2}}_{\mathrm{o,H_2}} - \dot{H}^{\mathrm{pre\_h_2}}_{\mathrm{i,H_2}}) \tag{60}$$

where the inlet enthalpy flow due to the exhaust fluid $\dot{H}^{\mathrm{pre\_h_2}}_{\mathrm{i,exh}}$ is an input coming from the afterburner, the inlet enthalpy flow due to the hydrogen fluid $\dot{H}^{\mathrm{pre\_h_2}}_{\mathrm{i,H_2}}$ equals $\dot{H}^{\mathrm{src}}_{\mathrm{H_2}}$ as shown in Fig. 16, and the outlet enthalpy flow of the hydrogen fluid $\dot{H}^{\mathrm{pre\_h_2}}_{\mathrm{o,H_2}}$ is the energy flowing to the SOFC anode $\dot{H}_{\mathrm{i,an}}$. Similar to (54), based on $\dot{n}^{\mathrm{pre\_h_2}}_{\mathrm{o,exh}}$ and $\dot{H}^{\mathrm{pre\_h_2}}_{\mathrm{o,exh}}$, the temperature of the exhaust fluid at the outlet of the hydrogen preheater $T^{\mathrm{pre\_h_2}}_{\mathrm{o,exh}}$ can be obtained according to:

$$\begin{aligned}\dot{H}^{\mathrm{pre\_h_2}}_{\mathrm{o,exh}} &= \dot{n}^{\mathrm{pre\_h_2}}_{\mathrm{o,exh}} \cdot \overline{h}_{\mathrm{exh}}(T^{\mathrm{pre\_h_2}}_{\mathrm{o,exh}}) \\ &= \dot{n}^{\mathrm{pre\_h_2}}_{\mathrm{o,exh}} \cdot \left(\overline{h}^{0}_{\mathrm{f,exh}} + \overline{c}_{\mathrm{p,exh}}(T^{\mathrm{pre\_h_2}}_{\mathrm{o,exh}} - T_0)\right)\end{aligned} \tag{61}$$

REFERENCES

[1] U. S. Department of Energy, "DOE hydrogen and fuel cells program: 2014 Annual Progress Report," U.S. Dept. Energy, Washington, DC, USA, Nov. 2014.

[2] M. H. Nehrir and C. Wang, *Modeling and Control of Fuel cells*. Piscataway, NJ, USA: Wiley/IEEE Press, 2009.

[3] L. Larminie and A. Dicks, *Fuel Cell Systems Explained*, 2nd ed. New York, NY, USA: Wiley, 2003.

[4] R. P. O'Hayre, S. W. Cha, W. Colella, and F. B. Prinz, *Fuel Cell Fundamentals*. New York, NY, USA: Wiley, 2006.

[5] M. C. Williams, J. P. Strakey, and S. C. Singhal, "U.S. distributed generation fuel cell program," *J. Power Sources*, vol. 131, no. 1, pp. 79–85, May 2004.

[6] T. Ota, M. Koyama, C. Wen, K. Yamada, and H. Takahashi, "Object-based modeling of SOFC system: Dynamic behavior of micro-tube SOFC," *J. Power Sources*, vol. 118, no. 1, pp. 430–439, May 2003.

[7] K. Kendall and M. Palin, "A small solid oxide fuel cell demonstrator for microelectronic applications," *J. Power Sources*, vol. 71, no. 1, pp. 268–270, Mar. 1998.

[8] H. W. Dommel, "Digital computer solution of electromagnetic transients in single-and multiphase networks," *IEEE Trans. Power App. Syst.*, vol. PAS-88, no. 4, pp. 388–399, Apr. 1969.
[9] A. M. Gole, O. B. Nayak, T. S. Sidhu, and M. S. Sachdev, "A graphical electromagnetic simulation laboratory for power systems engineering programs," *IEEE Trans. Power Syst.*, vol. 11, no. 2, pp. 599–606, May 1996.
[10] K. Strunz and E. Carlson, "Nested fast and simultaneous solution for time-domain simulation of integrative power-electric and electronic systems," *IEEE Trans. Power Del.*, vol. 22, no. 1, pp. 277–287, Jan. 2007.
[11] S. Filizadeh, M. Heidari, A. Mehrizi-Sani, J. Jatskevich, and J. Martinez, "Techniques for interfacing electromagnetic transient simulation programs with general mathematical tools IEEE taskforce on interfacing techniques for simulation tools," *IEEE Trans. Power Del.*, vol. 23, no. 4, pp. 2610–2622, Oct. 2008.
[12] V. Salehi, A. Mohamed, A. Mazloomzadeh, and O. A. Mohammed, "Laboratory-based smart power system—Part I: Design and system development," *IEEE Trans. Smart Grid*, vol. 3, no. 3, pp. 1394–1404, Sep. 2012.
[13] A. M. O. Haruni, M. Negnevitsky, M. E. Haque, and A. Gargoom, "A novel operation and control strategy for a standalone hybrid renewable power system," *IEEE Trans. Sustain. Energy*, vol. 4, no. 2, pp. 402–413, Apr. 2013.
[14] H. Aki *et al.* "Operational strategies of networked fuel cells in residential homes," *IEEE Trans. Power Syst.*, vol. 21, no. 3, pp. 1405–1414, Aug. 2006.
[15] S. Ziaeinejad, Y. Sangsefidi, and A. Mehrizi-Sani, "Fuel cell-based auxiliary power unit: EMS, sizing, and current estimator-based controller," *IEEE Trans. Veh. Technol.*, vol. 65, no. 6, pp. 4826–4835, Jun. 2016.
[16] A. Gebregergis, P. Pillay, D. Bhattacharyya, and R. Rengaswemy, "Solid oxide fuel cell modeling," *IEEE Trans. Ind. Electron.*, vol. 56, no. 1, pp. 139–148, Jan. 2009.
[17] K. Sedghisigarchi and A. Feliachi, "Dynamic and transient analysis of power distribution systems with fuel cells—Part I: Fuel-cell dynamic model," *IEEE Trans. Energy Convers.*, vol. 19, no. 2, pp. 423–428, Jun. 2004.
[18] E. Achenbach, "Response of a solid oxide fuel cell to load change," *J. Power Sources*, vol. 57, pp. 105–109, Sep.–Dec. 1995.
[19] S. Nagata, A. Momma, T. Kato, and Y. Kasuga, "Numerical analysis of output characteristics of tubular SOFC with internal reformer," *J. Power Sources*, vol. 101, no. 1, pp. 60–71, Oct. 2001.
[20] X. Xue, J. Tang, N. Sammes, and Y. Du, "Dynamic modeling of single tubular SOFC combining heat/mass transfer and electrochemical reaction effects," *J. Power Sources*, vol. 142, pp. 211–222, Mar. 2005.
[21] C. Wang and M. H. Nehrir, "A physically based dynamic model for solid oxide fuel cells," *IEEE Trans. Energy Convers.*, vol. 22, no. 4, pp. 887–897, Dec. 2007.
[22] M. D. Lukas, K. Y. Lee, and H. Ghezel-Ayagh, "An explicit dynamic model for direct reforming carbonate fuel cell stack," *IEEE Trans. Energy Convers.*, vol. 16, no. 3, pp. 289–295, Sep. 2001.
[23] R. Bird, W. Stewart, and E. Lightfoot, *Transport Phenomena*, 2nd ed. New York, NY, USA: Wiley, 2002.
[24] M. J. Moran, H. N. Shapiro, D. D. Boettner, and M. B. Bailey, *Fundamentals of Engineering Thermodynamics*. New York, NY, USA: Wiley, 2010.
[25] R. Bove and S. Ubertini, *Modeling Solid Oxide Fuel Cells*. Dordrecht, The Netherlands: Springer, 2008.
[26] K. Howe and K. Kendall, "Transient performance of micro-tubular solid oxide fuel cells and stacks," *ECS Trans.*, vol. 35, no. 1, pp. 419–423, 2011.
[27] Q. A. Huang, R. Hui, B. Wang, and J. Zhang, "A review of AC impedance modeling and validation in SOFC diagnosis," *Electrochim. Acta*, vol. 52, no. 28, pp. 8144–8164, Oct. 2007.
[28] S. H. Chan, C. F. Low, and O. L. Ding, "Energy and exergy analysis of simple solid-oxide fuel-cell power systems," *J. Power Sources*, vol. 103, no. 2, pp. 188–200, Feb. 2002.
[29] R. Gaynor, F. Mueller, F. Jabbari, and J. Brouwer, "On control concepts to prevent fuel starvation in solid oxide fuel cells," *J. Power Sources*, vol. 180, no. 1, pp. 330–342, May 2008.
[30] Y. H. Li, S. Rajakaruna, and S. S. Choi, "Control of a solid oxide fuel cell power plant in a grid-connected system," *IEEE Trans. Energy Convers.*, vol. 22, no. 2, pp. 405–413, Jun. 2007.
[31] R. Gemmen, "Analysis for the effect of inverter ripple current on fuel cell operating condition," *J. Fluids Eng.*, vol. 125, pp. 576–585, May 2003.
[32] S. Campanari and P. Iora, "Definition and sensitivity analysis of a finite volume SOFC model for a tubular cell geometry," *J. Power Sources*, vol. 132, no. 1, pp. 113–126, May 2004.
[33] C. M. Colson and M. H. Nehrir, "Evaluating the benefits of a hybrid solid oxide fuel cell combined heat and power plant for energy sustainability and emissions avoidance," *IEEE Trans. Energy Convers.*, vol. 26, no. 1, pp. 140–148, Mar. 2011.
[34] M. Dokiya, "SOFC system and technology," *Solid State Ionics*, vol. 152, pp. 383–392, Dec. 2002.

Tian Lan received the master's degree in control theory and control engineering from Tongji University, Shanghai, China, in 2011. He is currently working toward the Ph.D. degree with the Institute of Sustainable Electric Networks and Sources of Energy, Technische Universität Berlin, Berlin, Germany. His current research interests include fuel-cell-based combined heat and power systems.

Kai Strunz received the Dipl.-Ing. and Dr.-Ing. (*summa cum laude*) degrees from the Saarland University, Saarbrücken, Germany, in 1996 and 2001, respectively. From 1995 to 1997, he pursued research at Brunel University London, London, U.K. From 1997 to 2002, he worked at the Division Recherche et Développement of Electricité de France in the Paris area. From 2002 to 2007, he was an Assistant Professor of electrical engineering with the University of Washington in Seattle. Since September 2007, he has been Professor with the Institute of Sustainable Electric Networks and Sources of Energy, Technische Universität Berlin, Berlin, Germany.

Dr. Strunz is the Chairman of the IEEE Power and Energy Society (PES) Subcommittee on Distributed Energy Resources and the Chairman of the Subcommittee on Research in Education. He received the IEEE PES Prize Paper Award in 2015 and the IEEE JOURNAL OF EMERGING AND SELECTED TOPICS IN POWER ELECTRONICS First Prize Paper Award in 2015.